7-1-2014

Relationship Between Foveal Cone Specialization and Pit Morphology in Albinism

Melissa A. Wilk
Medical College of Wisconsin

John T. McAllister
Medical College of Wisconsin

Robert F. Cooper
Marquette University

Adam M. Dubis
University College London

Teresa N. Patitucci
Medical College of Wisconsin

See next page for additional authors

Accepted version. *Investigative Ophthalmology & Visual Science*, Vol. 55, No. 7 (July 2014): 4186-4198. DOI.

Authors
Melissa A. Wilk, John T. McAllister, Robert F. Cooper, Adam M. Dubis, Teresa N. Patitucci, Phyllis Summerfelt, Jennifer L. Anderson, Deborah M. Costakos, Thomas B. Connor Jr., William J. Wirostko, Pei-Wen Chiang, Alfredo Dubra, Christine A. Curcio, Murray H. Briliant, C. Gail Summers, Joseph Carroll, and Jennifer L. Anderson

Relationship between Foveal Cone Specialization and Pit Morphology in Albinism

Melissa A. Wilk
Department of Cell Biology, Neurobiology and Anatomy, Medical College of Wisconsin
Milwaukee, WI

John T. McAllister
Department of Ophthalmology, Medical College of Wisconsin
Milwaukee, WI

Robert F. Cooper
Department of Biomedical Engineering, Marquette University
Milwaukee, WI

Adam M. Dubis
Moorfields Eye Hospital
Institute of Ophthalmology, University College
London, United Kingdom

Teresa N. Patitucci
Department of Cell Biology, Neurobiology and Anatomy, Medical College of Wisconsin
Milwaukee, WI

Investigative Ophthalmology & Visual Science, Vol. 55, No. 7 (July 2014): pg. 4186-4198. DOI.

Phyllis Summerfelt

Department of Ophthalmology, Medical College of Wisconsin
Milwaukee, WI

Jennifer L. Anderson

Core Laboratory, Marshfield Clinic
Marshfield,WI

Kimberly E. Stepien

Department of Ophthalmology, Medical College of Wisconsin,
Milwaukee, WI

Deborah M. Costakos

Department of Ophthalmology, Medical College of Wisconsin,
Milwaukee, WI

Thomas B. Connor, Jr.

Department of Ophthalmology, Medical College of Wisconsin,
Milwaukee, WI

William J. Wirostko

Department of Ophthalmology, Medical College of Wisconsin,
Milwaukee, WI

Pei-Wen Chiang

Casey Eye Institute Molecular Diagnostics Laboratory
Portland, OR

Alfredo Dubra

Department of Ophthalmology, Medical College of Wisconsin
Department of Biomedical Engineering, Marquette University
Department of Biophysics, Medical College of Wisconsin,
Milwaukee, WI

Investigative Ophthalmology & Visual Science, Vol. 55, No. 7 (July 2014): pg. 4186-4198. DOI.

Christine A. Curcio
Department of Ophthalmology, University of Alabama School of Medicine
Birmingham, AL

Murray H. Brilliant
Center for Human Genetics, Marshfield Clinic
Marshfield, WI

C. Gail Summers
Departments of Ophthalmology and Visual Neurosciences and Pediatrics, University of Minnesota
Minneapolis, MN

Joseph Carroll
Department of Cell Biology, Neurobiology and Anatomy, Medical College of Wisconsin
Department of Ophthalmology, Medical College of Wisconsin
Department of Biomedical Engineering, Marquette University
Department of Biophysics, Medical College of Wisconsin, Milwaukee, WI

Abstract

Purpose.

Albinism is associated with disrupted foveal development, though intersubject variability is becoming appreciated. We sought to quantify this variability, and examine the relationship between foveal cone specialization and pit morphology in patients with a clinical diagnosis of albinism.

Investigative Ophthalmology & Visual Science, Vol. 55, No. 7 (July 2014): pg. 4186-4198. DOI.

Methods.

We recruited 32 subjects with a clinical diagnosis of albinism. DNA was obtained from 25 subjects, and known albinism genes were analyzed for mutations. Relative inner and outer segment (IS and OS) lengthening (fovea-to-perifovea ratio) was determined from manually segmented spectral domain-optical coherence tomography (SD-OCT) B-scans. Foveal pit morphology was quantified for eight subjects from macular SD-OCT volumes. Ten subjects underwent imaging with adaptive optics scanning light ophthalmoscopy (AOSLO), and cone density was measured.

Results.

We found mutations in 22 of 25 subjects, including five novel mutations. All subjects lacked complete excavation of inner retinal layers at the fovea, though four subjects had foveal pits with normal diameter and/or volume. Peak cone density and OS lengthening were variable and overlapped with that observed in normal controls. A fifth hyper-reflective band was observed in the outer retina on SD-OCT in the majority of the subjects with albinism.

Conclusions.

Foveal cone specialization and pit morphology vary greatly in albinism. Normal cone packing was observed in the absence of a foveal pit, suggesting a pit is not required for packing to occur. The degree to which retinal anatomy correlates with genotype or visual function remains unclear, and future examination of larger patient groups will provide important insight on this issue.

Keywords: albinism, adaptive optics, foveal morphology, foveal development

Introduction

Albinism is a group of inherited disorders characterized by absent or reduced melanin pigment in the eye, and often in the skin and hair. Although pigmentary manifestations of ocular albinism (OA1; MIM 300500, Xp22.3-Xp22.2) generally are limited to the eye, oculocutaneous albinism types 1A and 1B (OCA1; MIM 203100, mutations in *TYR*, 11q14.3) display features of completely absent (OCA1A) or near absent (OCA1B) systemic melanin expression.[1] Additionally, OCA2, OCA3, and OCA4 also have been described.[2,3] Ophthalmic manifestations of albinism include iris transillumination, macular translucency, photosensitivity, refractive errors, nystagmus,

absence of a foveal avascular zone, absence or incomplete formation of a foveal pit, loss of the annular reflex, impaired stereopsis, and altered retinostriate decussation. Most importantly, however, patients with all forms of albinism tend to have poor visual acuity despite refractive correction.[4,5] With the emergence of therapeutic strategies aimed at restoring vision in patients with albinism,[6–8] it is essential to clarify the relationship between the anatomical manifestations of the disease and functional deficits in these patients.

Previous studies have demonstrated variability in foveal morphology in subjects with albinism.[9–12] As demonstrated with spectral domain-optical coherence tomography (SD-OCT), foveal morphology in albinism can range from planar in appearance to a macula with increased thickening and even a shallow foveal depression. Thomas et al.[11] recently proposed a grading scheme for assessing the degree of foveal hypoplasia in subjects with albinism. Their grading scale defined normal structure as complete excavation of plexiform layers with presence of a foveal pit, as well as outer segment (OS) elongation and outer nuclear layer (ONL) widening at the fovea. Grade 1 hypoplasia displays all normal characteristics except complete excavation of the plexiform layers, while Grade 2 hypoplasia has no excavation of plexiform layers and no foveal pit, but residual OS elongation and ONL widening. Retinae with only ONL widening are classified as Grade 3 hypoplasia, and Grade 4 hypoplasia indicates that all aspects of normal foveal specialization are absent, resulting in relatively planar retinal thickness.

There is evidence that this variation in foveal morphology may be predictive of visual acuity,[11,12] though Chong et al.[13] found that subjects with suspected OA and nearly identical retinal findings had highly variable visual acuity. Additionally, Marmor et al.[10] showed that, in four subjects lacking foveal pits, the absence of a pit did not preclude central cone development or good visual acuity. Moreover, while these previous studies focused on the pit, other anatomical specializations are associated with the foveal region, most notably increased cone packing and elongation of the foveal cone outer segments.[14] Therefore, discrepancies in previous results regarding the role of foveal morphology in visual function may be due to an incomplete understanding of how foveal morphology relates to foveal cone specialization in patients with albinism.

While it is possible to assess foveal cone lengthening and ONL thickness using OCT, ONL measurements can be confounded by the presence of the Henle fiber layer,[15] obviating direct quantification of

Investigative Ophthalmology & Visual Science, Vol. 55, No. 7 (July 2014): pg. 4186-4198. DOI.

cone packing. Adaptive optics (AO) imaging, through correction of the eyes' monochromatic higher-order aberrations, enables visualization of rod and cone photoreceptors, and, thus, direct measurement of cone packing.[16–18] Two previous studies using flood-illuminated AO imaging demonstrated measureable cone packing in some subjects with albinism, even in those lacking a foveal pit.[9,10] However, neither study examined peak foveal cone density, leaving the question of how foveal cone specialization relates to foveal morphology in albinism unanswered. Here, we sought to assess directly foveal cone specialization (i.e., packing density and relative foveal-to-perifoveal lengthening) and foveal pit morphology in patients with a clinical diagnosis of albinism. Our results indicated the need for a modified foveal anatomical classification scheme in albinism, and served as a foundation for future studies examining structure-function and genotype-phenotype relationships in albinism.

Methods

Subjects

This study followed the tenets of the Declaration of Helsinki and was approved by the Children's Hospital of Wisconsin Institutional Review Board. After an explanation of the nature and possible consequences of the study, participants (or the adult guardian of minors) provided informed written consent. We recruited 32 subjects with a clinical diagnosis of albinism (19 male, 13 female; mean age ± SD = 23.9 ± 16.7 years) for this study (see Table). Supplementary Table S1 outlines which imaging was performed on each subject. The clinical diagnosis of albinism was based on features, such as the presence of iris transillumination, a positive angle κ, and/or misrouting of retinostriate fibers, in addition to abnormal retinal pigmentation (lack of peripheral melanin pigment in the RPE, presence or absence of macular coarsely granular melanin pigment). Patients diagnosed with OCA also displayed abnormal tanning due to the reduced or absent melanin in the skin. When possible, males with suspected OA1 also had the obligate carrier examined for pigmentary mosaicism. A total of 64 subjects with normal vision (38 male, 26 female; mean age ± SD = 26.8 ± 9.2 years) were recruited to serve as controls for various aspects of this study.

Investigative Ophthalmology & Visual Science, Vol. 55, No. 7 (July 2014): pg. 4186-4198. DOI.

Grade	Subject	Sex	Age	Eye	Axial Length, mm	Phenotype	Genotype	Visual Acuity	Plexiform Excavation	Normal*			
										Foveal Pit	IS Ratio	OS Ratio	ONL Widening
1a	JC_0131	M	20	OD	24.94	OCA2	*OCA2* c.2228C>T; p.743Pro>Leu	20/40+†	N	Y	Y	Y	Y
	JC_0140	M	11	OD	22.06	OCA1B	No variants found‡	20/20−3†	N	Y	Y	Y	Y
	JC_0456	M	17	OD	23.62	OCA2	*OCA2* c.1327G>A; p.443Val>Ile & c.1555delG (FS), *TYRP1* c.1103delA (FS)	20/60−2§	N	Y	Y	Y	Y
	KS_0935	M	7	OD	20.77	OCA1	*TYR* c.1217C>T; p.406Pro>Leu & c.961T>C; p.321Cys>Arg‖	20/40§	N	Y	Y	Y	Y
1b	JC_0170	F	16	OD	23.84	OCA1B	No sample	20/40†	N	Shallow	Y	Y	Y
	JC_0492	F	28	OD	23.62	OCA1B	*TYR* c.1147G>A; p.383Asp>Asn & c.1217C>T; p.406Pro>Leu	20/25†	N	Shallow	Y	Y	Y
	JC_0493	F	21	OD	22.33	OCA1B	*TYR* c.1147G>A; p.383Asp>Asn & c.1217C>T; p.406Pro>Leu	20/20−†	N	Shallow	Y	Y	Y
	JC_0598	M	9	OD	23.64	OCA2	*OCA2* c.1327G>A; p.443Val>Ile	20/60−2§	N	Shallow	Y	Y	Y
	JC_6813	M	8	OD	21.07	OCA	No sample	NA	N	Shallow	N	Y	Y
	WW_0592	F	55	OD	23.24	OCA1	*TYR* c.1217C>T; p.406Pro>Leu	20/70§	N	Shallow	Y	Y	Y
2	DC_0831	M	7	OD	21.38	OCA1	*TYR* c.1467_1468insT (FS)	20/40−2§	N	N	Y	Y	Y
	JC_0125	M	28	OD	22.49	OCA1B	No variants found¶	20/60†	N	N	Y	Y	Y
	JC_0494	M	10	OS	21.13	OCA2	*OCA2* c.1465A>G; p.489Asn>Asp & c.868A>G; p.290Arg>Gly	20/80−†	N	N	Y	Y	Y
	JC_0829	F	10	OD	21.43	OCA1	*TYR* c.899A>C; p.300Asn>Thr‖ & c.1217C>T; p.406Pro>Leu & c.1467_1468insT (FS)	20/200§	N	N	Y	Y	Y
	JC_6809	M	61	OD	25.13	OCA	No sample	NA	N	N	N	Y	Y
	JC_10074	F	17	OS	23.54	OCA2	*OCA2* c.365C>T; p.122Thr>Ile & c.2207C>T; p.736Ser>Leu	20/70 −2§	N	N	Y	Y	Y
3	AD_0063	M	32	OD	24.33	OA1	*GPR143* exon 1 deletion	20/60§	N	N	Y	N	Y
	AD_0065	M	31	OD	25.40	OA1	No sample; brother to AD_0063	NA	N	N	Y	N	Y
	JC_0150	F	25	OD	27.20	OCA2	*OCA2* c.1441G>A; p.481Ala>Thr	20/70−†	N	N	Y	N	Y
	JC_0156	F	11	OD	21.68	OCA1A	*TYR* c.1118C>A; p.373Thr>Lys	20/70†	N	N	Y	N	Y
	JC_0157	M	13	OD	23.27	OCA1A	*TYR* c.1118C>A; p.373Thr>Lys	20/70†	N	N	Y	N	Y
	JC_0174	M	19	OS	24.12	OA1	*GPR143* c.933C>A; p.311Tyr>Stop	20/70†	N	N	Y	N	Y
	JC_0438	M	23	OD	21.05	OCA4	*SLC45A2* c.264delC (FS) & c.1417G>A; p.473Gly>Ser‖	20/70†	N	N	Y	N	Y
	JC_0459	F	21	OD	23.90	OCA	No variants found**	20/80+§	N	N	N	N	Y
	JC_6811	F	16	OD	21.88	OCA	No sample	NA	N	N	Y	N	Y
	JC_10073	F	20	OD	22.34	OCA1	*TYR* c.976C>T; p.325Gln>Stop (homozygous)	20/125§	N	N	Y	N	Y
	KS_0551	M	31	OD	24.94	OA1	*GPR143* c.112G>A; p.38Gly>Arg‖	20/100§	N	N	Y	N	Y
4	JC_0103	M	20	OD	22.58	OA1	*GPR143* c.797T>C; p.266Leu>Pro‖	20/80†	N	N	Y	N	N
	JC_0421	F	24	OD	22.42	OCA1	No variants found††	NA	N	N	Y	N	N
	JC_0442	M	83	OD	23.08	OCA2	*OCA2* c.2228C>T; p.743Pro>Leu (homozygous)	20/80†	N	N	N	N	N
	JC_6804	F	43	OD	20.42	OCA	No sample	NA	N	N	N	N	N
	JC_6807	M	27	OD	23.39	OCA	No sample	NA	N	N	Y	N	N

Eye, eye used for axial length, BCVA, and foveal metrics; OD, right; OS, left; FS, frameshift; NA, not available.
* Normal is defined as being within 2 SDs of the average of the normal population.
† Best-corrected visual acuity.
‡ Following genes were examined: *TYR* (all exons), *OCA2* (all translated exons), *TYRP1* (all translated exons), *SLC45A2* (all exons), and *GPR143* (all exons except exon 1).
§ Visual acuity with correction.
‖ Novel mutation.
¶ Following genes were examined: *TYR* (all exons except exons 2, 4, and 5), *OCA2* (all translated exons except exons 6, 10, 12, 16, 18-21, and 23-24).
** Following genes were examined: *TYR* (all exons), *OCA2* (all translated exons, 2.7 kb deletion), *TYRP1* (all translated exons), and *SLC45A2* (all exons).
†† Following genes were examined: *TYR* (all exons), *OCA2* (all translated exons), *TYRP1* (all translated exons), and *SLC45A2* (all exons except exon 6).

Table 1 Summary of Subjects With Albinism

Genetic Testing

DNA was isolated from blood or saliva samples for 25 of the subjects with albinism at Marshfield Clinic Research Foundation and/or Casey Eye Institute for genetic analysis. Based on phenotype, patients were evaluated for mutations in the *TYR*, *OCA2*, *TYRP1*, *SLC45A2* (OCA1, OCA2, OCA3, and OCA4, respectively), and/or *GPR143* genes (OA1) by Sanger sequencing as described previously.[3,19–23] In addition, patients of African descent were screened for the previously identified 2.7 kb *OCA2* deletion.[24] DNA sequences were aligned and analyzed for mutations using DNASTAR Lasergene software (DNASTAR, Inc., Madison, WI, USA). Identified mutations were compared to the Albinism Database (available in the public domain at http://albinismdb.med.umn.edu/) to determine novelty.

SD-OCT Study

Volumetric images of the macula were acquired in 25 of 32 subjects with albinism and all 64 normal controls using the Zeiss Cirrus High Definition (HD)-OCT (Cirrus HD-OCT; Carl Zeiss Meditec, Dublin,

Investigative Ophthalmology & Visual Science, Vol. 55, No. 7 (July 2014): pg. 4186-4198. DOI.

CA, USA). Volume scans were nominally 6 × 6 mm and consisted of 128 B-scans (512 A-scans/B-scan). These scans were used to derive estimates of foveal pit morphology as described below. In addition, high-resolution SD-OCT (Bioptigen, Research Triangle Park, NC, USA) imaging was performed on all subjects. These scans were used for evaluation of the relative lengthening of the foveal cones as described below. The seven subjects with albinism for whom macular volumes were not obtained were imaged using the hand-held Bioptigen Envisu SD-OCT (Bioptigen). For both Bioptigen systems, line scan sets were acquired (750-1000 A-scans/B-scan, 100–200 repeated B-scans, nominal scan width of 6-8 mm) through the foveal center. When no pit was present, imaging was centered at the expected foveal center. Scans were registered and averaged as described previously to reduce speckle noise in the image.[25] For all devices, the lateral image dimension was linearly corrected for axial length. The assumed axial length was 24.46 and 24 mm for the Cirrus and Bioptigen devices, respectively. The corrected image width was calculated as the nominal scan width divided by the assumed axial length times the actual axial length.

Foveal Pit Morphology.

Using individual OCT line scans (Bioptigen), we graded each of the 32 subjects with albinism according to the foveal hypoplasia grading scale proposed by Thomas et al.,[11] as summarized in the Introduction. In addition, we quantified pit morphology in 64 control subjects and the eight subjects with albinism having Grade 1 foveal hypoplasia using volumetric SD-OCT scans (Cirrus HD-OCT; Carl Zeiss Meditec). Subject JC_0598 had significant nystagmus that prohibited accurate measurement, and JC_6813 had no available volumetric scan for measurement. As such, these subjects were unable to be assessed quantitatively for pit metrics. We used a modified version of our previously described algorithm,[26,27] which allows for differences in pit height on each side of the foveal pit for a given radial slice. This modification allowed for a better fit of the data to the difference of Gaussians than previous versions.

Measuring Relative Foveal Cone Inner and Outer Segment Lengthening.

Processed line scans for all 32 subjects with albinism were segmented manually at the anterior boundary of the inner limiting membrane (ILM), posterior boundary of the outer plexiform layer

Investigative Ophthalmology & Visual Science, Vol. 55, No. 7 (July 2014): pg. 4186-4198. DOI.

(OPL), center of the external limiting membrane (ELM), center of the ellipsoid zone (EZ), center of the interdigitation zone (IZ), and posterior edge of the RPE-Bruch's Membrane (RPE-BrM) band. As previously described,[9] the segmented layers then were interpolated, and layer thicknesses were extracted using custom software (Matlab; Mathworks, Natick, MA, USA). Inner segment (IS) and OS thickness was taken as the ELM-EZ distance and the EZ-IZ distance, respectively. The IS and OS values were binned and averaged at 0.1 mm increments between 2 mm nasal and 2 mm temporal to the fovea. The relative foveal-to-perifoveal lengthening then was calculated by dividing the foveal IS (or OS) thickness value by the average of the IS (or OS) thickness at 1.75 mm nasal and temporal. For one subject (WW_0592), the ratios were calculated using the foveal thickness relative to the nasal peripheral value only, as the temporal retina showed significant outer retinal disruption. These data then were compared to previously published normative data from 167 subjects (72 males, 95 females; mean age = 32.6 years).[9]

Adaptive Optics Scanning Light Ophthalmoscopy (AOSLO)

The AOSLO method was used to obtain images of the photoreceptor mosaic in 10 subjects with albinism (5 male, 5 female; mean age ± SD = 21 ± 13.9 years) and nine control subjects (7 male, 2 female; mean age ± SD = 25 ± 4.5 years). Before imaging, one drop each of phenylephrine hydrochloride (2.5%) and tropicamide (1%) were used to dilate the pupil and suspend accommodation in the eye of interest. Images were obtained using a variable field-of-view, which ranged from 1° × 1° to 2° × 2°. Individual raw image sequences contained between 150 and 200 frames, and an adjustable internal fixation target was used to obtain images at and around the expected location of the fovea as well as along a temporal strip extending to the perifovea. Following image acquisition, each image sequence was processed as previously described to generate a high signal-to-noise ratio image from each image sequence.[28,29] These processed images were aligned to create a montage using commercial software (Adobe Photoshop; Adobe Systems, Inc., San Jose, CA, USA).

AOSLO Cone Density.

Cone density was analyzed using the processed AOSLO images. To ensure the measurements across subjects were acquired relative to a common anatomical feature, we used peak cone density as the

Investigative Ophthalmology & Visual Science, Vol. 55, No. 7 (July 2014): pg. 4186-4198. DOI.

reference point for each subject. Peak cone density was determined by first cropping a large area of the montage at the expected foveal center. Every cone in this image then was identified using a semiautomated cone identification algorithm.[30] We measured cone density at each pixel in the image using each of 10 sampling windows ranging in size from 25 × 25 to 45 × 45 μm. The 10 densities for each pixel were averaged to create an average density map. The location of peak density in this average density map was used as the location of peak density for subsequent analysis of the overall montage. This minimized the effect of local inhomogeneities of the cone mosaic. With this location determined, cone density was measured using a 37 × 37 μm sampling window (comparable size to that used by Curcio et al.[31]) at the location of peak density and each of 16 additional regions of interest (0.5, 0.65, 1.0, 1.5, 2.0, 3.0, 4.0, 5.0, 6.0, 7.0, 8.0, 9.0, 10.0, 12.0, 15.0, and 20.0 degrees relative to the location of peak cone density in the temporal direction). Not all locations could be assessed for each subject due to poor image quality or incomplete montages. Images within 2° of the location of peak density were counted again using the semiautomated program.[30] Locations beyond 2° were manually counted by a single observer (MAW) using ImageJ (Wayne Rasband, National Institutes of Health [NIH], Bethesda, MD; available in the public domain at http://rsb.info.nih.gov/ij/index.html) due to the presence of rod photoreceptors.

Results

Genetic Results

Of the 25 subjects for whom DNA was analyzed, 23 distinct mutations (total of 34 mutations) were found in 22 of the subjects (see Table). Five of the mutations have not been reported previously to our knowledge and are considered novel (*GPR143* c.112G>A, p.38Gly>Arg; *GPR143* c.797T>C, p.266Leu>Pro; *TYR* c.961T>C, p.321Cys>Arg; *TYR* c.899A>C, p.300Asn>Thr; and *SLC45A2* c.1417G>A, p.473Gly>Ser). The likely pathogenicity was determined using SIFT, PolyPhen-2, and PROVEAN analysis tools. The SIFT (version 1.03 available in the public domain at http://sift.jcvi.org/, accessed September 2013) results are reported to be tolerated if tolerance index > 0.05 or damaging if tolerance index ≤ 0.05. PolyPhen-2 (version 2.2.2, available in the public domain at http://genetics.bwh.harvard.edu/pph2/, accessed September 2013) appraises mutations qualitatively as benign, possibly damaging (POS) or probably damaging (PRD) based on the model's false-positive rate.

Investigative Ophthalmology & Visual Science, Vol. 55, No. 7 (July 2014): pg. 4186-4198. DOI.

The PROVEAN (version 1.1, available in the public domain at http://provean.jcvi.org/human_protein_batch_submit.php, accessed September 2013) results are reported as having a neutral or deleterious effect as determined by averaged δ alignment scores. Analysis yielded the following results: *GPR143* p.266Leu>Pro, *TYR* p.321Cys>Arg, and *SLC45A2* p.473Gly>Ser were found to be damaging, probably damaging, and deleterious by the three analysis tools; *TYR* p.300Asn>Thr was found to be damaging, possibly damaging, and deleterious; *GPR143* c.112G>A, p.38Gly>Arg was considered to be tolerated, benign, and neutral by these tools, though similar mutations of nearby amino acids (p.35Gly>Asp and p.39Leu>Arg) result in the OA1 phenotype, suggesting this may, in fact, be a causative mutation. Consistent with previous results, no mutations were found in 12% of our tested subjects with albinism, reflecting the likely role of other, unidentified genes in albinism.[2,32–34]

Foveal Pit Morphology in Albinism Can Overlap With Normal Variation

Analysis of the 64 control subjects shows that normal foveal pit morphology is highly variable, consistent with previous studies.[27,35] Normal pit depth ranged from 0.035 to 0.176 mm (average ± SD = 0.118 ± 0.029 mm), pit diameter ranged from 1.06 to 2.50 mm (average ± SD = 1.87 ± 0.24 mm), and pit volume ranged from 0.021 to 0.230 mm^3 (average ± SD = 0.085 ± 0.038 mm^3). Though all of our subjects with albinism lacked complete excavation of inner retinal layers (Fig. 1), four of our subjects had pits within 2 SDs of the normal average depth, diameter, and/or volume (Figs. 2A–D). Subject JC_0456 had normal pit volume (0.013 mm^3), KS_0935 had normal pit diameter and volume (1.70 mm and 0.030 mm^3, respectively), JC_0131 had normal pit diameter and volume (1.71 mm and 0.027 mm^3, respectively), and JC_0140 had normal pit diameter and volume (1.68 mm, and volume of 0.014 mm^3, respectively). In addition, KS_0935 had a foveal pit that was deeper than that of one of the normal controls, further demonstrating overlap between the normal and albinotic distributions.

Investigative Ophthalmology & Visual Science, Vol. 55, No. 7 (July 2014): pg. 4186-4198. DOI.

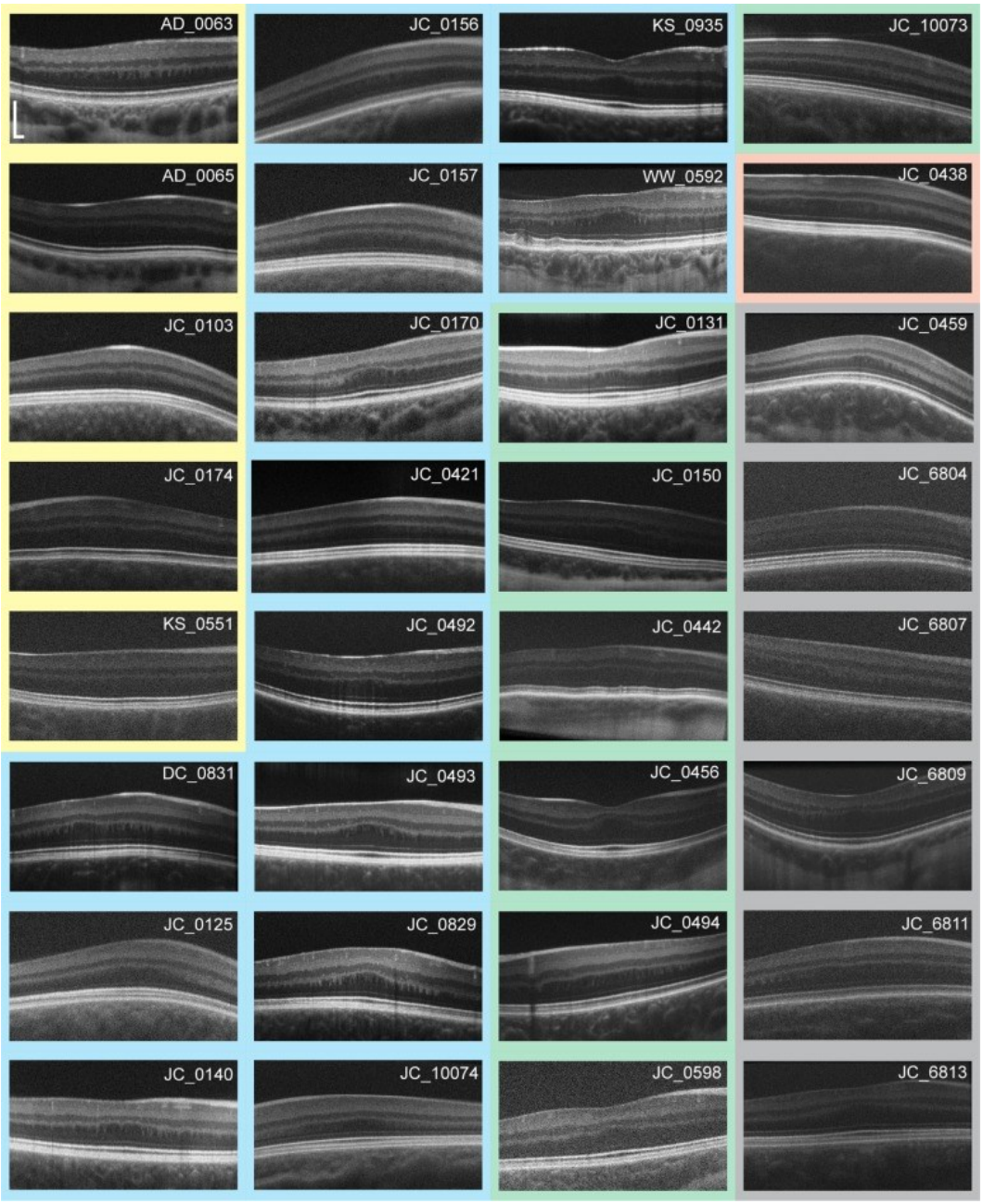

Figure 1 Variability in foveal morphology in albinism. The SD-OCT horizontal line scans through the expected foveal location are shown for all subjects with albinism, grouped by clinical diagnosis (phenotype). *Yellow*, OA1; *blue*, OCA1; *green*, OCA2; *orange*, OCA4; and *gray*, OCA with unspecified type. *Scale bar*: 200 μm for all subjects.

Investigative Ophthalmology & Visual Science, Vol. 55, No. 7 (July 2014): pg. 4186-4198. DOI.

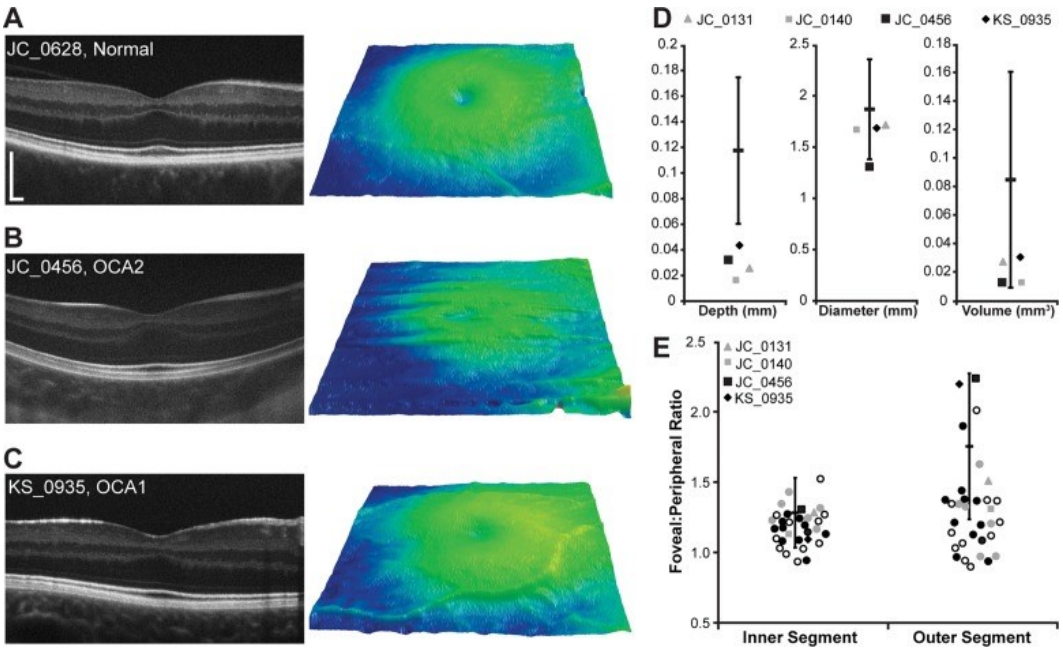

Figure 2 Foveal morphology in albinism can overlap with normal values. (**A**–**C**) *Left panel* is a high-resolution SD-OCT horizontal line scan image acquired through the fovea. *Scale bar*: 200 µm for all subjects. *Right panel* shows macular thickness maps centered on the fovea. (**A**) Subject JC_0628 represents a control subject with a shallow foveal pit with incomplete excavation of the inner retinal layers. (**B**, **C**) Subjects JC_0456 (OCA2) and KS_0935 (OCA1) are subjects with albinism who have well-defined foveal pits. (**D**, **E**) *Open symbols* represent the subjects with no genetic mutations identified, *filled gray symbols* represent the subjects with one mutation identified, *filled black symbols* represent subjects with 2 or more mutations or hemizygous mutations, and *circles* represent subjects with pit metrics outside 2 SDs of the normal mean or no measurable pit. (**D**) Quantification of foveal pit depth, diameter, and volume. The *black bar* represents the mean of 64 control subjects, and the *error bars* represent ±2 SDs. Four subjects with albinism had at least one aspect of their foveal pit morphology (depth, diameter, and/or volume) within 2 SDs of the normal mean. (**E**) The distribution of IS and OS ratios for all 32 subjects with albinism relative to 167 control subjects (the *black bar* is the previously published mean of 167 control subjects, and the *error bars* represent ±2 SDs[9]). No differences in IS or OS lengthening were seen between subjects with no mutations and those with 1 or more mutations (P = 0.37 for IS and P = 0.34 for OS; Mann-Whitney U test).

Relative Foveal-to-Peripheral Cone Lengthening Varies in Albinism

The relative lengthening of cone IS and OS at the fovea, defined as the ratio of the foveal IS (or OS) length to the perifoveal IS (or OS) length, is highly variable in subjects with albinism (mean ± SD = 1.18 ± 0.13 for IS and 1.32 ± 0.35 for OS). As shown in Figure 2E, these values partially overlap with the degree of foveal cone lengthening previously reported for 167 controls subjects (mean ± SD = 1.283 ±

Investigative Ophthalmology & Visual Science, Vol. 55, No. 7 (July 2014): pg. 4186-4198. DOI.

0.125 for IS and 1.757 ± 0.261 for OS).[9] Moreover, 16 of the 32 subjects with albinism had OS ratios within 2 SDs of the normal mean. When comparing IS and OS lengthening in subjects with no mutations to those with one or more mutations, there were no significant differences between groups (P = 0.37 for IS and P = 0.34 for OS; Mann-Whitney U test), providing evidence that the subjects lacking genetic verification of albinism are not different from subjects with identified mutations.

Here, we have shown that these specializations can occur in the absence of a fully-developed foveal pit. The four subjects with albinism who had normal pits also showed normal cone IS and OS foveal-to-perifoveal lengthening. However, even in subjects who lacked a normal pit, 23 of 28 had normal IS foveal-to-perifoveal lengthening, and 12 of 28 had normal foveal-to-perifoveal OS lengthening. This supports the thought that cone OS elongation is not dependent on the presence of a foveal pit.

Normal Foveal Cone Packing Can Occur in Albinism

Peak cone density in our nine control subjects ranged from 84,733 to 165,080 cones/mm^2 (average ± SD = 130,508 ± 23,968 cones/mm^2), consistent with previous results.[31,36,37] Peak cone density in the 10 subjects with albinism we assessed also was variable, ranging from 29,218 to 126,370 cones/mm^2 (average ± SD = 80,496 ± 27,185 cones/mm^2, Fig. 3). While on average this is below normal, the two distributions clearly overlap. Moreover, all but two of the subjects with albinism showed cone density topography that was similar in shape to that seen in the normal retina (i.e., a precipitous fall off in cone density as a function of eccentricity). Subject JC_0103 showed little to no packing, with a peak cone density of only 29,218 cones/mm^2. This planar topography is consistent with results reported previously for this subject using flood-illuminated AO imaging.[9] In addition, JC_10074 had a reduced peak density (44,558 cones/mm^2) with a rather slow fall-off, though packing still is evident. Cone density as a function of eccentricity for all subjects is shown in Figure 4. Statistical analysis of peak cone densities from subjects with one identified mutation in *TYR* shows that they are not significantly different from subjects with two or more mutations of *TYR* (P = 0.86, Wilcoxon rank sum test).

Investigative Ophthalmology & Visual Science, Vol. 55, No. 7 (July 2014): pg. 4186-4198. DOI.

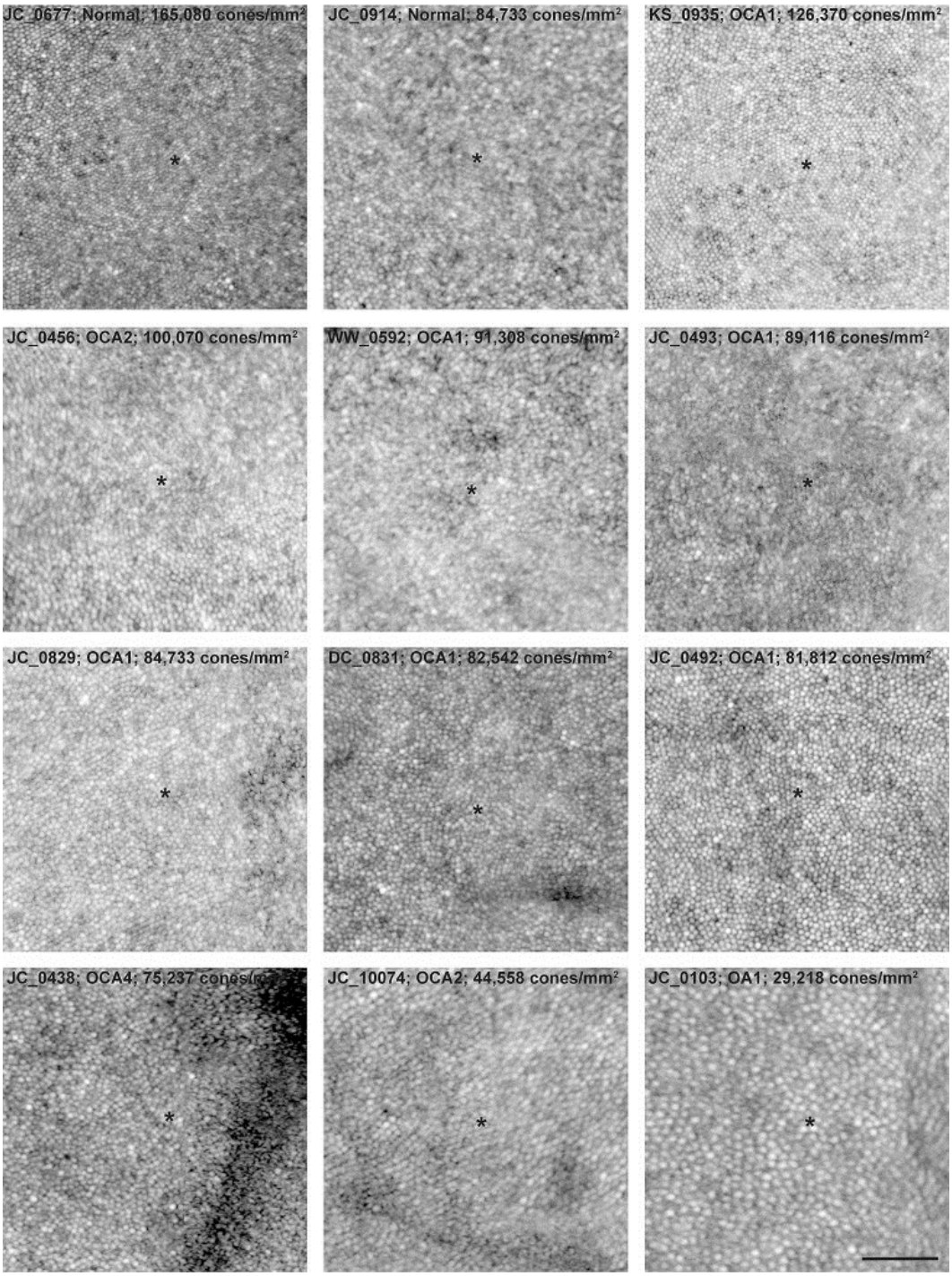

Figure 3 Visualizing foveal cone packing in albinism. Montages of the central retina surrounding the location of peak cone density (*) are shown using a logarithmic display for 10 subjects with albinism and two normal controls. Qualitatively, it can be seen that cone density decreases (larger, more coarsely packed cells) moving away from the location of peak density for all subjects except JC_0103, whose cone mosaic

Investigative Ophthalmology & Visual Science, Vol. 55, No. 7 (July 2014): pg. 4186-4198. DOI.

appears to have larger cones and uniform packing across the central retina. No significant differences in peak cone density were seen between subjects with one *TYR* mutation and those with two or more *TYR* mutations (P = 0.86, Wilcoxon rank sum test). *Scale bar*: 50 μm for all subjects.

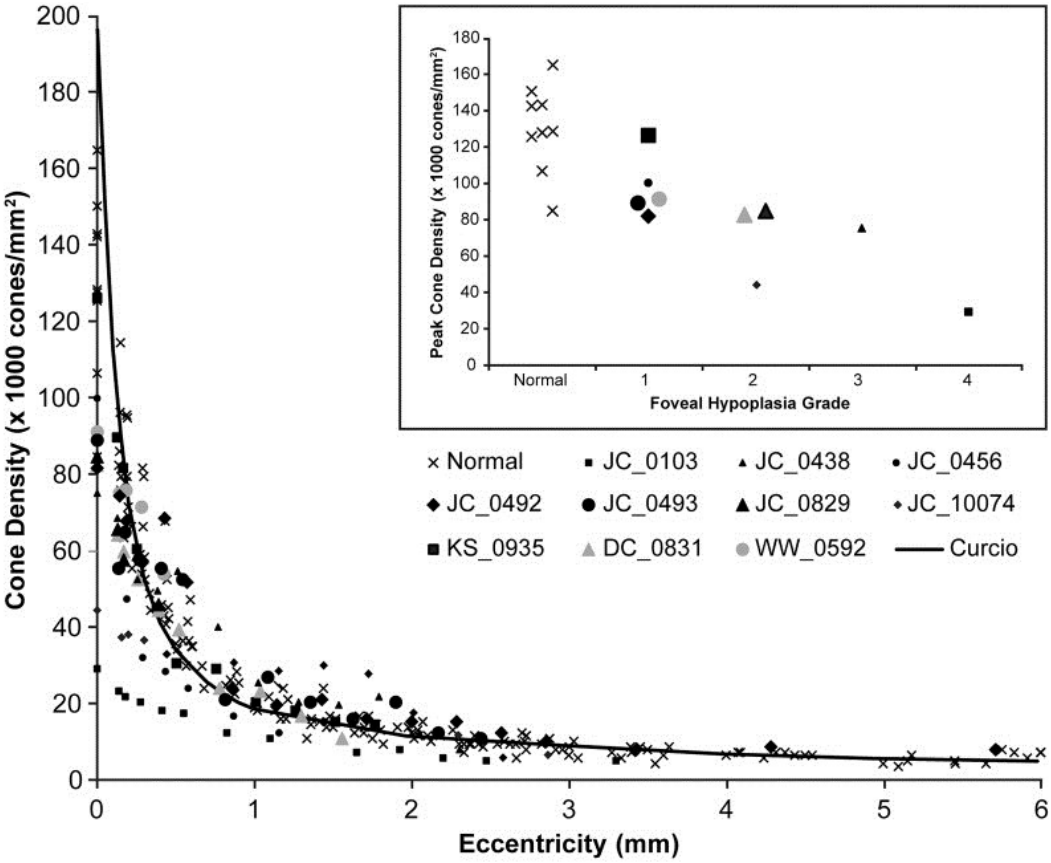

Figure 4 Quantifying foveal cone packing in albinism. Cone density is plotted over a range of eccentricities (0 being the location of peak cone density) for 10 subjects with albinism, nine control subjects (x), and normative data from Curcio et al. (*black line*).[31] For the subjects with albinism, *filled black symbols* represent subjects with 2 or more mutations or hemizygous mutations, *filled gray symbols* represent subjects with 1 mutation. Though some subjects with albinism appear to have lower absolute peak cone densities, all show a prominent increase in cone density at the fovea, with the exception of JC_0103 and JC_10074. *Inset*: Peak cone density versus degree of foveal hypoplasia using the grading scheme of Thomas et al.[11] Subjects with more normal foveal morphology (i.e., lower grade of foveal hypoplasia) tend to have higher peak cone density.

We did not observe a link between cone density and visual acuity. For example, subjects with similar visual acuity (WW_0592, JC_0438, and JC_0103; visual acuities of 20/70, 20/70, and 20/80, respectively) had dramatically different peak cone densities (91,308, 75,237, and 29,218 cones/mm^2, respectively). In addition, one subject

Investigative Ophthalmology & Visual Science, Vol. 55, No. 7 (July 2014): pg. 4186-4198. DOI.

with albinism who had normal peak cone density had significantly reduced visual acuity (JC_0456, peak density = 100,070 cones/mm^2, visual acuity with correction = 20/60^{-2}). These data indicated that foveal cone density alone may not be the limiting factor for visual function in albinism.

Foveal Cone Packing Is Not Pit-Dependent

Subjects with a lower grade of foveal hypoplasia as defined by the grading scheme of Thomas et al.[11] tended to have higher peak cone densities than subjects with less-developed foveae, and the two subjects with the greatest degree of inner retinal excavation had normal peak cone densities (Fig. 4, inset). This suggested that, though the pit is not required for packing to occur, the presence of a pit may facilitate or augment cone packing at the fovea. Interestingly, JC_0103 has genetically-confirmed OA1 and had the lowest peak cone density (whereas the other 9 subjects all were OCA). However, due to our small sample size, it remains to be seen to what extent cone packing is dictated by genotype.

Resolving a Fifth Hyper-Reflective Band in Albinism

Upon evaluation of the high-resolution SD-OCT line scans, we observed the presence of a fifth hyper-reflective band in the outer retina of several subjects with albinism. To verify these visual observations, we created longitudinal reflectivity profiles (LRP) for each of these subjects as well as our 64 control subjects using ImageJ (Wayne Rasband, NIH). The LRPs were measured at the expected fovea as well as a perifoveal location comparable to those locations examined by Spaide and Curcio.[38] We then evaluated the LRP plots to determine the number of peaks (hyper-reflective bands) in the outer retina. As reviewed by Spaide and Curcio,[38,39] the normal outer retina typically contains four hyper-reflective bands corresponding to the ELM, EZ, IZ, and RPE-BrM, and we also observed these 4 bands in the majority of our normal population (Fig. 5A). However, in 24 of our 32 subjects with albinism, the singular RPE-BrM band seen in the normal retina was split into two bands, resulting in a fifth hyper-reflective band in the outer retina (Figs. 5C, C,5D).5D). This "extra" band is significantly more prevalent among subjects with albinism ($P <$ 0.0001, Fisher's exact test), having been seen in only seven of our control subjects (Fig. 5B).

Investigative Ophthalmology & Visual Science, Vol. 55, No. 7 (July 2014): pg. 4186-4198. DOI.

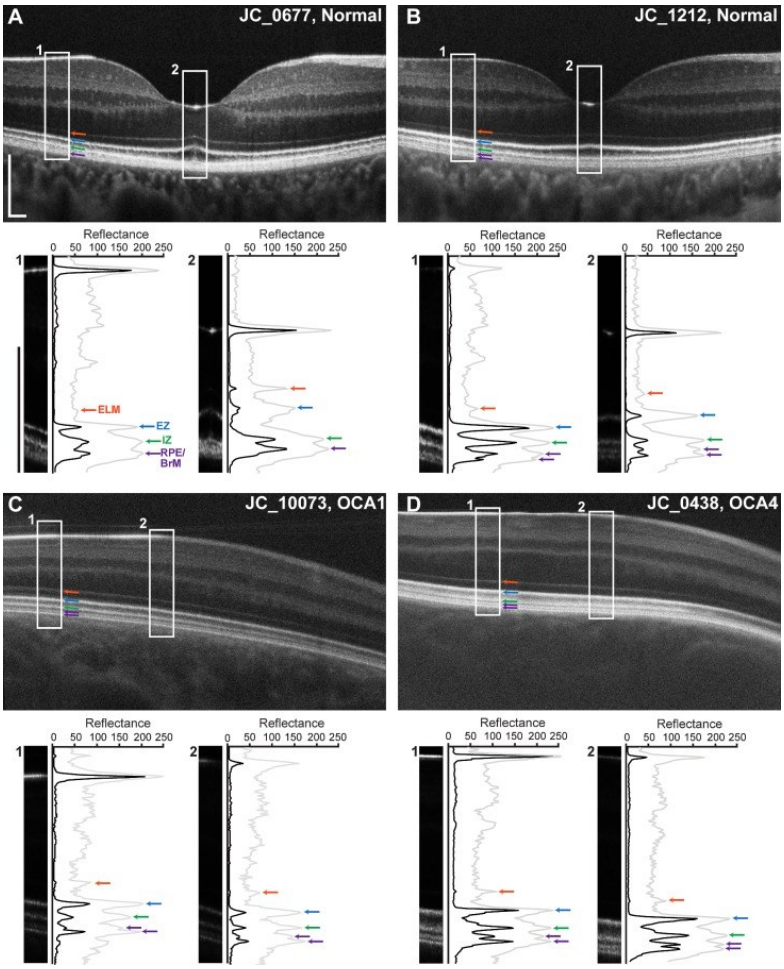

Figure 5 Altered appearance of the outer retinal hyper-reflective SD-OCT bands in albinism. (**A**–**D**) *Top* shows a logarithmic high-resolution horizontal line scan. *Arrows* indicate the nomenclature of Spaide and Curcio[38] given to the outer retinal hyper-reflective bands: *orange*, ELM; *blue*, EZ; *green*, IZ; *purple*, RPE and BrM. *Scale bars* = 200 µm. *White boxes* (263 × 345 µm) delineate the areas of each image that are analyzed in the *bottom*. The *bottom* shows an LRP analysis for the central five pixels of the image excerpts (linear format) to the *left* of each plot. The *gray line* is the LRP for the logarithmic image, and the *black line* is the LRP for the linear image. Faint ELM bands are lost in the linear LRP, but the presence of a fifth hyper-reflective band is illustrated clearly in the linear LRP. *Arrows* in the *bottom* are color-matched to the image in the *top* to show the respective peaks for each hyper-reflective band. (**A**) Subject JC_0677 is a representative normal subject with a total of four outer retinal hyper-reflective bands at foveal and perifoveal locations. (**B**) Subject JC_1212 is one of seven control subjects (of 64 analyzed control subjects) with a fifth hyper-reflective band (denoted by the *second purple arrow*). (**C**, **D**) Representative subjects with albinism (JC_10073 and JC_0438) also display the presence of a fifth hyper-reflective band in the outer retina. The presence of a fifth band is more prevalent in subjects with albinism than in the normal population ($P < 0.0001$, Fisher's exact test).

Investigative Ophthalmology & Visual Science, Vol. 55, No. 7 (July 2014): pg. 4186-4198. DOI.

Discussion

Toward Quantitative Classification of Foveal Morphology in Albinism

The recently proposed grading scheme for assessing the degree of foveal hypoplasia in subjects with albinism and other conditions relies on qualitative interpretation of foveal specialization.[11] Here, we used quantitative measurement of OS foveal-to-perifoveal lengthening to differentiate Grades 1 and 2 from Grades 3 and 4, and this objective approach should permit more standardized grading. In addition, we quantified foveal pit morphology in our subjects having Grade 1 hypoplasia and found that some of these subjects had foveal pit morphology within normal limits, contrary to the classic clinical picture of albinism. Thus, we propose to distinguish two subsets of Grade 1 hypoplasia based on quantitative analysis of foveal pit morphology: Grade 1a, in which normal pit metrics (depth, diameter, and/or volume within 2 SDs of the normal average) are observed, and Grade 1b, in which the pit is only a shallow indent (depth, diameter, and volume outside 2 SDs of the normal average). Differentiation of Grade 3 from Grade 4 could be possible using quantitative measurement of ONL widening; however, the orientation of Henle fibers may be disrupted in albinism, complicating accurate segmentation of the ONL. Further refinement of grading the macular phenotype in albinism could include peak cone density, though this was not done due to the small number of subjects for whom peak cone density was assessed.

The Relationship Between Cone Packing and Pit Morphology: Implications for Models of Foveal Development

The ability to assess foveal cone density directly provides an opportunity to probe the relationship between pit morphology and cone packing. This relationship has been a somewhat controversial topic in models of foveal development, and two distinct models have evolved to describe this interaction—the passive and the active. Passive models predict that the foveal pit is developed first through mechanical forces; namely, a relative increase in intraocular pressure (IOP), acting on the foveal avascular zone (FAZ), and cone packing is a passive result of lifting forces induced by retinal stretch at the foveal pit.[40–43] Conversely, active models suggest that molecular gradients result in active elongation of cone photoreceptors at the fovea, and

Investigative Ophthalmology & Visual Science, Vol. 55, No. 7 (July 2014): pg. 4186-4198. DOI.

cohesion of neighboring photoreceptors results in cone inner segments being drawn toward the foveal center.[14,44] This mechanism accounts for cone displacements that take place throughout the macular region before the foveal pit develops[45,46] and suggests that perinatal remodeling of the pit is due to a variety of factors, including the local predominance of midget cell circuits, and has the adaptive advantage of thinning the retina and relocating foveal neurons closer to a blood supply on the foveal rim.[14,44]

Though evidence has shown that cone packing can occur in the absence of a developed foveal pit,[9–11] our present cone density data also suggest a role for the pit in determining the degree of cone packing. Of the 10 subjects with albinism analyzed here, the two subjects with albinism who had the most developed pits had peak cone densities within normal limits, and those with less developed pits had progressively decreasing peak cone densities (Fig. 4, inset). Therefore, our data supported a hybrid model incorporating passive and active components to foveal development. With substantial packing occurring in the absence of a pit, we propose that the active model of cone packing is responsible for initial packing, resulting in cone density that ultimately is less than the final peak cone density for normal adults. Following initial elongation and packing, a depression of inner retina (i.e., the early foveal pit) forms most likely as a result of mechanical factors (e.g., a relative increase in IOP at the FAZ). Subsequently, growth-induced stretch generates the lifting forces that promote further elongation and centripetal displacement of cone inner segments toward the fovea. This additional displacement of cones would result in the elevated peak cone density that is seen in normal adults and is lacking in subjects without a foveal pit. This hybrid "active-passive" model better fits our data than either model alone.

Functional Consequences of Variable Foveal Specialization

With our current data, some conclusions can be made about the relationships between pit morphology, cone specialization, and visual function. Though generally better visual acuity is associated with lower grades of foveal hypoplasia (consistent with previous data[11,12]), some of our subjects with albinism had near normal foveal morphology, but relatively poor visual acuity, supporting previous claims that foveal morphology alone is not an accurate predictor of visual function.[10,13] Moreover, some of our subjects with normal cone OS elongation and/or normal cone packing still had poor visual acuity (as poor as

Investigative Ophthalmology & Visual Science, Vol. 55, No. 7 (July 2014): pg. 4186-4198. DOI.

20/200). This suggests that visual acuity in these subjects is not solely limited by peak foveal cone density. One explanation for this is based on data from Rossi and Roorda,[47] who showed that at eccentricities near the center of fixation, the Nyquist limit of the cone mosaic predicts the minimum angle of resolution, whereas visual resolution outside the fovea is not limited by the cones but by the midget retinal ganglion cell (mRGC) mosaic due to convergence of photoreceptors onto postreceptoral cells. Additionally, Provis et al.[14] have suggested that the formation of a fovea is reliant on the fact that most midget bipolar cells within the foveal region connect to a single cone and a single mRGC. The presence of nonconvergent pathways facilitates displacement of mRGCs in response to foveogenic forces.[14] Thus, it is possible that in the absence of a true fovea, as in albinism, the preferred retinal locus of fixation (PRLF) does not have the nonconvergent pathway, thereby prohibiting the excavation of the inner retinal layers.[14] As such, the mRGC Nyquist limit would be the true predictor of visual acuity across the retina, including at the PRLF and area of peak cone density. Therefore, differences in cone-RGC pathways may explain differences in visual acuity seen in subjects that have nearly identical cone densities.

A Band Divided: Insight Into SD-OCT Layer Nomenclature

Typically, four outer retinal hyper-reflective bands are observed in OCT images, which currently are being identified as the ELM, EZ, IZ, and RPE-BrM.[38,39] Our normative perifoveal OCT data match that detailed by Spaide and Curcio.[38] These four bands also are distinguishable in our subjects with albinism, suggesting that melanosomes, whether in the RPE cell body or in the apical processes, are not required for a third band signal. This, in turn, implies that the OS tips (and surrounding interphotoreceptor matrix) are, indeed, a reflectivity source in themselves, as many investigators posit.[48–50] Differences in OCT images between controls and subjects with albinism, however, do exist. Namely, there is a prominent hyporeflective band between the IZ and RPE-BrM bands and a splitting of the RPE-BrM, resulting in a fifth hyper-reflective band in the outer retina. While Srinivasan et al.[50] also have reported additional bands in the outer retina, these were located more anteriorly than our observed band, and were proposed to represent the rod and cone outer segments tips (ROST and COST). By contrast, the combination of the fourth and fifth bands with the intervening hyporeflective band

Investigative Ophthalmology & Visual Science, Vol. 55, No. 7 (July 2014): pg. 4186-4198. DOI.

appears to fill the space occupied by the RPE-BrM band seen in normal retinae.

The melanosomes serve to absorb photons, while their physical properties cause increased light scatter, contributing to the single, large hyper-reflective OCT band in most control subjects (RPE-BrM). When melanin is reduced, as in albinism, a fifth hyper-reflective band appears because reduced light scatter, visualized as an absence of hyper-reflectivity in the center of the RPE-BrM band, apparently unmasks independent reflectivity sources internal and external to it. Why a fifth band also is seen in some of our control subjects is unclear, though variability in RPE melanin[51,52] across subjects could be a contributing factor.

It is possible that the fifth hyper-reflective band actually is a visualization of Bruch's membrane, separate from the RPE, as suggested previously.[38,50,53] In this case, the hyporeflective band that unmasks a hyper-reflective BrM band might be attributable to basal infoldings of the RPE plasma membrane. These specializations maximize the surface area for exchange[54] and are more prominent in younger adults than older adults.[55] Because albinism results in retinal underdevelopment, it is plausible that these immature retinae also include increased basal RPE infoldings. However, we see no correlation between the hyporeflective band, the level of foveal development, or age up to sixth decade in our subjects with albinism. Alternatively, the fifth band may represent specializations with independent reflectivity contributions inside vertically compartmentalized RPE.[56–58] These include mitochondria in the basolateral third of the cells, as mitochondria are hypothesized optical elements for photoreceptors.[38,59] Use of AO-OCT,[60–62] with improved lateral and axial resolution, in subjects with albinism may allow further delineation of these newly revealed bands. Examination of older subjects with albinism in the age range of basal infolding reduction (60+ years) and more precise information about RPE organelle compartmentalization[58] also will help address these questions.

Conclusions

We have shown a wide range of foveal morphology and foveal cone specialization in subjects with albinism. These foveal characteristics can overlap with those seen in normal retinae, challenging the presumption that foveal hypoplasia (or foveal plana) is a universal phenotype in patients with albinism. We concluded,

Investigative Ophthalmology & Visual Science, Vol. 55, No. 7 (July 2014): pg. 4186-4198. DOI.

however, that while a foveal pit is not required for foveal cone specialization, it may facilitate further cone packing. In addition, we found that the presence of normal foveal characteristics (developed pit, elongation of foveal cone OS, cone packing) does not necessarily result in normal visual acuity. Thus, it will be important to consider other factors (e.g., nystagmus[63–65] and cortical organization[66–69]) when evaluating the therapeutic potential of a given patient, with those patients having more significant retinal contributions to their overall phenotype being perhaps better responders to therapies aimed at altering retinal anatomy. Finally, the degree to which the anatomical manifestations of albinism vary across genotypes remains unresolved and will have a crucial role in the development and targeting of therapeutic strategies.

Acknowledgments

The authors thank Michael McGowan at the National Organization for Albinism and Hypopigmentation (NOAH), Phil Sommer, Eric Buckland, and Sunita Suyarem for their contributions to this work, as well as Jan Provis for her thoughtful insight and discussion.

Supported by NIH Grants T32EY014537, P30EY001931, R01EY017607, and R01EY006109; Thomas M. Aaberg, Sr., Retina Research Fund; Vision for Tomorrow; EyeSight Foundation of Alabama; and unrestricted departmental grants from Research to Prevent Blindness, Inc., New York, NY, USA, to the Department of Ophthalmology at the Medical College of Wisconsin, the Department of Ophthalmology and Visual Neurosciences at the University of Minnesota, and the Department of Ophthalmology at the University of Alabama School of Medicine. This investigation was conducted in a facility constructed with support from Research Facilities Improvement Program, Grant Number C06-RR016511, from the National Center for Research Resources, NIH. Also supported by a Career Award at the Scientific Interface from the Burroughs Wellcome Fund and a Career Development Award from Research to Prevent Blindness (AD). Partially supported by the National Center for Advancing Translational Sciences, NIH, through Grants UL1TR000427 and UL1TR000055. The authors alone are responsible for the content and writing of the paper.

Disclosure: **M.A. Wilk**, None; **J.T. McAllister**, None; **R.F. Cooper**, None; **A.M. Dubis**, None; **T.N. Patitucci**, None; **P. Summerfelt**, None; **J.L. Anderson**, None; **K.E. Stepien**, None; **D.M. Costakos**, None; **T.B. Connor Jr**, None; **W.J. Wirostko**, None; **P.-W. Chiang**,

Investigative Ophthalmology & Visual Science, Vol. 55, No. 7 (July 2014): pg. 4186-4198. DOI.

None; **A. Dubra**, Canon, Inc. (C); **C.A. Curcio**, None; **M.H. Brilliant**, None; **C.G. Summers**, None; **J. Carroll**, Carl Zeiss Meditec (F), Bioptigen, Inc. (S)

References

1. King RA, Pietsch J, Fryer JP, et al. Tyrosinase gene mutations in oculocutaneous albinism 1 (OCA1): definition of the phenotype. *Hum Genet*. 2003; 113: 502–513
2. Oetting WS, King RA. Molecular basis of albinism: mutations and polymorphisms of pigmentation genes associated with albinism. *Hum Mutat*. 1999; 13: 99–115
3. Newton JM, Cohen-Barak O, Hagiwara N, et al. Mutations in the human orthologue of the mouse underwhite gene (uw) underlie a new form of oculocutaneous albinism, OCA4. *Am J Hum Genet*. 2001; 69: 981–988
4. Oetting WS, Summers CG, King RA. Albinism and the associated ocular defects. *Metab Pediatr Syst Ophthalmol*. 1994; 17: 5–9
5. Summers CG. Vision in albinism. *Trans Am Ophthalmol Soc*. 1996; 94: 1095–1155
6. Onojafe IF, Adams DR, Simeonov DR, et al. Nitisinone improves eye and skin pigmentation defects in a mouse model of oculocutaneous albinism. *J Clin Invest*. 2011; 121: 3914–3923
7. Struck MC. Vision response to dopamine replacement. NCT01663935. 2012. Available at http://clinicaltrials.gov/show/NCT01663935
8. Summers CG. Trial of L-DOPA as a treatment to improve vision in albinism. NCT01176435. 2010. Available at http://clinicaltrials.gov/ct2/show/NCT01176435
9. McAllister JT, Dubis AM, Tait DM, et al. Arrested development: high-resolution imaging of foveal morphology in albinism. *Vision Res*. 2010; 50: 810–817
10. Marmor MF, Choi SS, Zawadzki RJ, Werner JS. Visual insignificance of the foveal pit: reassessment of foveal hypoplasia as fovea plana. *Arch Ophthalmol*. 2008; 126: 907–913
11. Thomas MG, Kumar A, Mohammad S, et al. Structural grading of foveal hypoplasia using spectral-domain optical coherence tomography a predictor of visual acuity? *Ophthalmology*. 2011; 118: 1653–1660
12. Seo JH, Yu YS, Kim JH, Choung HK, Heo JW, Kim SJ. Correlation of visual acuity with foveal hypoplasia grading by optical coherence tomography in albinism. *Ophthalmology*. 2007; 114: 1547–1551
13. Chong GT, Farsiu S, Freedman SF, et al. Abnormal foveal morphology in ocular albinism imaged with spectral-domain optical coherence tomography. *Arch Ophthalmol*. 2009; 127: 37–44
14. Provis JM, Dubis AM, Maddess T, Carroll J. Adaptation of the central retina for high acuity vision: cones, the fovea, and the avascular zone. *Prog Retin Eye Res*. 2013; 35: 63–81
15. Lujan BJ, Roorda A, Knighton RW, Carroll J. Revealing Henle's fiber layer using spectral domain optical coherence tomography. *Invest Ophthalmol Vis Sci*. 2011; 52: 1486–1492

Investigative Ophthalmology & Visual Science, Vol. 55, No. 7 (July 2014): pg. 4186-4198. DOI.

16. Chui TYP, Song HX, Burns SA. Individual variations in human cone photoreceptor packing density: variations with refractive error. *Invest Ophthalmol Vis Sci*. 2008; 49: 4679–4687
17. Rossi EA, Chung M, Dubra A, Hunter JJ, Merigan WH, Williams DR. Imaging retinal mosaics in the living eye. *Eye*. 2011; 25: 301–308
18. Dubra A, Sulai Y, Norris JL, et al. Non-invasive imaging of the human rod photoreceptor mosaic using a confocal adaptive optics scanning ophthalmoscope. *Biomed Opt Express*. 2011; 2: 1864–1876
19. Garrison NA, Yi Z, Cohen-Barak O, et al. P gene mutations in patients with oculocutaneous albinism and findings suggestive of Hermansky-Pudlak syndrome. *J Med Genet*. 2004; 41: e86
20. Giebel LB, Strunk KM, Spritz RA. Organization and nucleotide sequences of the human tyrosinase gene and a truncated tyrosinase-related segment. *Genomics*. 1991; 9: 435–445
21. Lee ST, Nicholls RD, Jong MTC, Fukai K. Spritz RA. organization and sequence of the human P gene and identification of a new family of transport proteins. *Genomics*. 1995; 26: 354–363
22. Schiaffino MV, Bassi MT, Galli L, et al. Analysis of the OA1 gene reveals mutations in only one-third of patients with X-linked ocular albinism. *Hum Mol Genet*. 1995; 4: 2319–2325
23. Manga P, Kromberg JG, Box NF, Sturm RA, Jenkins T, Ramsay M. Rufous oculocutaneous albinism in southern African Blacks is caused by mutations in the TYRP1 gene. *Am J Hum Genet*. 1997; 61: 1095–1101
24. Durham-Pierre D, Gardner JM, Nakatsu Y, et al. African origin of an intragenic deletion of the human P gene in tyrosinase positive oculocutaneous albinism. *Nat Genet*. 1994; 7: 176–179
25. Tanna H, Dubis AM, Ayub N, et al. Retinal imaging using commercial broadband optical coherence tomography. *Br J Ophthalmol*. 2010; 94: 372–376
26. Dubis AM, McAllister JT, Carroll J. Reconstructing foveal pit morphology from optical coherence tomography imaging. *Br J Ophthalmol*. 2009; 93: 1223–1227
27. Dubis AM, Hansen BR, Cooper RF, Beringer J, Dubra A, Carroll J. Relationship between the foveal avascular zone and foveal pit morphology. *Invest Ophthalmol Vis Sci*. 2012; 53: 1628–1636
28. Cooper RF, Dubis AM, Pavaskar A, Rha J, Dubra A, Spatial Carroll J. and temporal variation of rod photoreceptor reflectance in the human retina. *Biomed Opt Express*. 2011; 2: 2577–2589
29. Dubra A, Harvey Z. Registration of 2D images from fast scanning ophthalmic instruments. In: Fischer B, Dawant BM, Lorenz C, editors. ed *The 4th International Workshop on Biomedical Image Registration*. Lübeck, Germany: Springer-Verlag Berlin, Heidelberg; 2010: 60–71
30. Garrioch R, Langlo C, Dubis AM, Cooper RF, Dubra A, Carroll J. Repeatability of in vivo parafoveal cone density and spacing measurements. *Optom Vis Sci*. 2012; 89: 632–643
31. Curcio CA, Sloan KR, Kalina RE, Hendrickson AE. Human photoreceptor topography. *J Comp Neurol*. 1990; 292: 497–523

Investigative Ophthalmology & Visual Science, Vol. 55, No. 7 (July 2014): pg. 4186-4198. DOI.

32. Hutton SM, Spritz RA. A comprehensive genetic study of autosomal recessive ocular albinism in Caucasian patients. *Invest Ophthalmol Vis Sci*. 2008; 49: 868–872
33. Preising MN, Forster H, Gonser M, Lorenz B. Screening of TYR, OCA2, GPR143, and MC1R in patients with congenital nystagmus, macular hypoplasia, and fundus hypopigmentation indicating albinism. *Mol Vis*. 2011; 17: 939–948
34. Sengupta M, Sarkar D, Mondal M, Samanta S, Sil A, Ray K. Analysis of MC1R variants in Indian oculocutaneous albinism patients: highlighting the risk of skin cancer among albinos. *J Genet*. 2013; 92: 305–308
35. Wagner-Schuman M, Dubis AM, Nordgren RN, et al. Race- and sex-related differences in retinal thickness and foveal pit morphology. *Invest Ophthalmol Vis Sci*. 2010; 52: 625–634
36. Li KY, Tiruveedhula P, Roorda A. Intersubject variability of foveal cone photoreceptor density in relation to eye length. *Invest Ophthalmol Vis Sci*. 2010; 51: 6858–6867
37. Gao H, Hollyfield JG. Aging of the human retina: differential loss of neurons and retinal pigment epithelial cells. *Invest Ophthalmol Vis Sci*. 1992; 33: 1–17
38. Spaide RF, Curcio CA. Anatomical correlates to the bands seen in the outer retina by optical coherence tomography: literature review and model. *Retina*. 2011; 31: 1609–1619
39. Spaide RF. Questioning optical coherence tomography. *Ophthalmology*. 2012; 119: 2203–2204
40. Springer AD. New role for the primate fovea: a retinal excavation determines photoreceptor deployment and shape. *Vis Neurosci*. 1999; 16: 629–636
41. Springer AD, Hendrickson AE. Development of the primate area of high acuity. 1. Use of finite element analysis models to identify mechanical variables affecting pit formation. *Vis Neurosci*. 2004; 21: 53–62
42. Springer AD, Hendrickson AE. Development of the primate area of high acuity. 2: quantitative morphological changes associated with retinal and pars plana growth. *Vis Neurosci*. 2004; 21: 775–790
43. Springer AD, Hendrickson AE. Development of the primate area of high acuity. 3: temporal relationships between pit formation, retinal elongation and cone packing. *Vis Neurosci*. 2005; 22: 171–185
44. Provis JM, Diaz CM, Dreher B. Ontogeny of the primate fovea: a central issue in retinal development. *Prog Neurobiol*. 1998; 54: 549–581
45. Diaz-Araya C, Provis JM. Evidence of photoreceptor migration during early foveal development: a quantitative analysis of human fetal retinae. *Vis Neurosci*. 1992; 8: 505–514
46. Cornish EE, Hendrickson AE, Provis JM. Distribution of short-wavelength-sensitive cones in human fetal and postnatal retina: early development of spatial order and density profiles. *Vision Res*. 2004; 44: 2019–2026
47. Rossi EA, Roorda A. The relationship between visual resolution and cone spacing in the human fovea. *Nat Neurosci*. 2010; 13: 156–157

Investigative Ophthalmology & Visual Science, Vol. 55, No. 7 (July 2014): pg. 4186-4198. DOI.

48. Zawadzki R, Cense B, Zhang Y, Choi S, Miller D, Werner JS. Ultrahigh-resolution optical coherence tomography with monochromatic and chromatic aberration correction. *Opt Express*. 2008; 16: 8126–8143
49. Götzinger E, Pircher M, Geitzenauer W, et al. Retinal pigment epithelium segmentation by polarization sensitive optical coherence tomography. *Opt Express*. 2008; 16: 16410–16422
50. Srinivasan VJ, Monson BK, Wojtkowski M, et al. Characterization of outer retinal morphology with high-speed, ultrahigh-resolution optical coherence tomography. *Invest Ophthalmol Vis Sci*. 2008; 49: 1571–1579
51. Weiter JJ, Delori FC, Wing GL, Fitch KA. Retinal pigment epithelial lipofuscin and melanin and choroidal melanin in human eyes. *Invest Ophthalmol Vis Sci*. 1986; 27: 145–152
52. Schmidt SY, Peisch RD. Melanin concentration in normal human retinal pigment epithelium: regional variation and age-related reduction. *Invest Ophthalmol Vis Sci*. 1986; 27: 1063–1067
53. Bloom SM, Singal IP. The outer Bruch membrane layer: a previously undescribed spectral-domain optical coherence tomography finding. *Retina*. 2011; 31: 316–323
54. Heriot WJ, Orlin C, Henkind P. Basal infolding density in the normal pigmented rat. *Ophthalmology*. 1986; 93: 484–486
55. Hogan MJ. Role of the retinal pigment epithelium in macular disease. *Trans Am Acad Ophthalmol Otolaryngol*. 1972; 76: 64–80
56. Hogan MJ, Alvarado J, Weddell J. *Histology of the Human Eye*. Philadelphia, PA: W.B. Saunders Company; 1971.
57. Krebs W, Krebs I. *Primate Retina and Choroid: Atlas of Fine Structure in Man and Monkey*. New York, NY: Springer-Verlag New York, Inc.; 1991.
58. Woodell A, Coughlin B, Kunchithapautham K, et al. Alternative complement pathway deficiency ameliorates chronic smoke-induced functional and morphological ocular injury. *PloS One*. 2013; 8: e67894
59. Hoang QV, Linsenmeier RA, Chung CK, Curcio CA. Photoreceptor inner segments in monkey and human retina: mitochondrial density, optics, and regional variation. *Vis Neurosci*. 2002; 19: 395–407
60. Torti C, Považay B, Hofer B, et al. Adaptive optics optical coherence tomography at 120,000 depth scans/s for non-invasive cellular phenotyping of the living human retina. *Opt Express*. 2009; 17: 19382–19400
61. Kocaoglu OP, Cense B, Jonnal RS, et al. Imaging retinal nerve fiber bundles using optical coherence tomography with adaptive optics. *Vision Res*. 2011; 51: 1835–1844
62. Kocaoglu OP, Lee S, Jonnal RS, et al. Imaging cone photoreceptors in three dimensions and in time using ultrahigh resolution optical coherence tomography with adaptive optics. *Biomed Opt Express*. 2011; 2: 748–763
63. Piling RF, Thompson JR, Gottlob I. Social and visual function in nystagmus. *Br J Ophthalmol*. 2005; 89: 1278–1281

Investigative Ophthalmology & Visual Science, Vol. 55, No. 7 (July 2014): pg. 4186-4198. DOI.

64. Abadi RV, Bjerre A. Motor and sensory characteristics of infantile nystagmus. *Br J Ophthalmol*. 2002; 86: 1152–1160
65. Fu VLN, Bilonick RA, Felius J, Hertle RW, Birch EE. Visual acuity development of children with infantile nystagmus syndrome. *Invest Ophthalmol Vis Sci*. 2011; 52: 1404–1411
66. von dem Hagen E, Hoffmann MB, Morland AB. Identifying human albinism: a comparison of VEP and fMRI. *Invest Ophthalmol Vis Sci*. 2008; 49: 238–249
67. von dem Hagen EA, Houston GC, Hoffmann MB, Morland AB. Pigmentation predicts the shift in the line of decussation in humans with albinism. *Eur J Neurosci*. 2007; 25: 503–511
68. von dem Hagen EAH, Houston GC, Hoffman MB, Jeffery G, Morland AB. Retinal abnormalities in human albinism translate into a reduction of grey matter in the occipital cortex. *Eur J Neurosci*. 2005; 22: 2475–2480
69. Hoffmann MB, Tolhurst DJ, Moore AT, Morland AB. Organization of the visual cortex in human albinism. *J Neurosci*. 2003; 23: 8921–8930

Investigative Ophthalmology & Visual Science, Vol. 55, No. 7 (July 2014): pg. 4186-4198. DOI.